Vortex-Antivortex Annihilation and Flux Turbulence in Layered Type-II Superconductors

E.E. Dvash · I. Shapiro · B. Rosenstein ·
N. Logoboy · B.Y. Shapiro

Abstract New mechanism of turbulence instability of standing flux-antiflux front in layered superconductors is presented. We describe two assisting mechanisms destabilizing the standing vortex-antivortex front. There are anisotropy of the layered superconductors and the heat, released by the vortex-antivortex annihilation. We present the conditions of the front stability for various anisotropy and heating parameters. We predict that heat released by the vortex-antivortex annihilations enhances the turbulence instability in superconductors with small anisotropy. The characteristic size of the unstable pattern is estimated. The results are in a good agreement with recent experiments.

Keywords Flux Instability · Anisotropic superconductors · Spatial pattern

1 Introduction

Studies of patterns in the magnetic flux distribution in the type-II superconductors are attracting the attention of many research groups [1–4] whose magneto-optical experiments demonstrate that nonuniform flux penetration occurs. Patterns with branch-like structures have been found in most of high T_c materials, like $YBa_2Cu_3O_{7-x}$ [5] and $Bi_2Sr_2CaCu_2O_{8+x}$ [6]. The nucleation of dendrite like patterns in MgB_2 films is another example [7, 8]. These complex structures consist of alternating low and high vortex density regions and are found in a certain temperature window. Likewise, flux penetration in the form of droplets separating areas of different densities of vortices has been observed in $NbSe_2$ [9]. Usually the occurrence of flux patterns in interfacial

E.E. Dvash · I. Shapiro · N. Logoboy · B.Y. Shapiro (✉)
Department of Physics, Institute of Superconductivity, Bar-Ilan University, Ramat-Gan 52900, Israel
e-mail: shapib51@hotmail.com

B. Rosenstein
Department of Electrophysics, National Chiao Tung University, Hsinchu, Taiwan, ROC

growth phenomena can be attributed to a diffusion driven, long-wavelength instability of a straight front, similar to the Mullins-Sekerka instability [10] found in crystal growth. The nucleation of nonuniform patterns associated with the propagation of a flux front into a flux-free sample has been attributed to such an interfacial instability. This results from a thermomagnetic coupling [7, 8, 11–13] where a higher temperature leads to a higher vortex mobility, enhanced flux flow, and hence a larger heat generation.

On the other hand, the situation when the vortices interact in a superconductor with the flux of the opposite sign is less theoretically studied. This flux configurations arises for example when a DC bias current creates vortices and antivortices on the opposite side of the superconducting strip [14]. Another example which is now under intensive investigation arises upon exposing the previously magnetized sample to the magnetic field of an opposite direction. Vlasko-Vlasov et al. [1] argued that the remagnetization flux front in platelet-shaped superconductors leads to formation of a specific three-dimensional structure inside the sample. This structure called "Meissner hole" consists of flux-free regions around which closed vortex loops are formed that sustain a local increase of current while, the boundary between vortices and antivortices exhibits a long wavelength instability [1, 2, 4, 15, 16]. The cause of the instability at the boundary between fluxes of opposite sign is still being debated. In particular Fisher et. al. [17, 18], proposed a non thermomagnetic Kelvin-Helmholtz mechanism of instability caused by an in-plane anisotropy of the vortex mobility [19]. This mechanism of instability was carefully reinvestigate by the van Saarloos [20] et al. They confirmed the finding of Fisher et al. [17, 18] that standing vortex-antivortex fronts have an instability for large anisotropy, while the moving fronts were found to be stable for all anisotropies. Several years latter this model was improved by an additional assumption of a step shape and anisotropy of the voltage current characteristics [18] and explained the experimental results in moderate anisotropic superconductor $YBa_2Cu_3O_{7-\delta}$. Unfortunately this assumption cannot explain the instability in pure isotropic systems like Nb and MgB_2 and recently discovered slightly anisotropic $Ba(Fe_{1-x}Co_x)_2As_2$ [21].

In the present paper we propose another mechanism of the turbulence instability showing that the heat released by the vortex-antivortex annihilations at the flux-antiflux front can create the Meissner holes and enhance the Kelvin-Helmholtz mechanism of the turbulence even in layered superconductors with small anisotropy.

2 Model and Basic Equations

We consider a thick film (slab) with sizes L in the y-direction and D in the x-direction, subjected to the oppositely directed magnetic field H (z-direction) at the sample edges. The field creates vortices and antivortices penetrating the sample and annihilating in the center of the film (Fig. 1). Electromagnetically the film is not thin in the Pearl sense, (namely the thickness in our case does not obey $d \ll \lambda$), so the relation between the current density and the magnetic induction is local [22]. We exploit a model of two-component vortex gas [23] spatially homogeneous along the z axes, which is valid for the experimentally interesting situation of the low magnetic field

Fig. 1 (**a**) Two-dimensional cross section of the sample in the XY plane, ϑ is the angle between the x axis and the ab plain of the layered structure and c axis is perpendicular to the layers of the superconductor. (**b**) Geometry of the sample
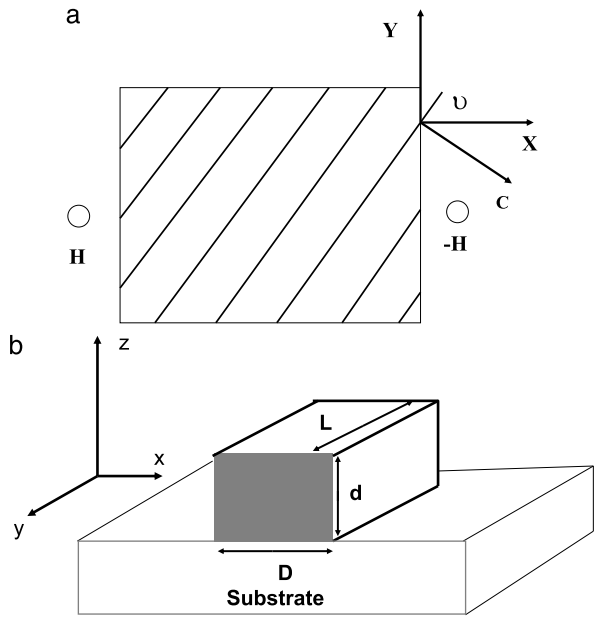
when typical spacing between vortices a_0 essentially exceeds vortex-vortex (antivortex) interaction radius ξ, and the vortex velocity depends only on the edge screening current that is assumed to be homogeneously distributed across the sample. One must take into account both vortex-antivortex annihilation and heat release accompanying this process. We should also take into consideration heat absorption by the sample lattice in order to prevent the rise of unlimited temperature.

The vortex-antivortex annihilation obeys the well-known master equations of the recombination theory [24, 25], see Appendix 1 for derivation,

$$\frac{\partial n_+}{\partial t} + \nabla(n_+\mathbf{v}_+) + gn_+n_- = 0, \tag{1}$$

$$\frac{\partial n_-}{\partial t} + \nabla(n_-\mathbf{v}_-) + gn_+n_- = 0, \tag{2}$$

$$g = \xi v, \quad v = \text{mod}(\mathbf{v}_+ - \mathbf{v}_-), \tag{3}$$

where n_+ and n_- are the vortex and antivortex densities, respectively, g is the ratio of recombination for vortices and antivortices, ξ is the cross section of the annihilation, which is of the order of the coherence length of the superconductor [26], and $\mathbf{v}_\pm$ are the opposite directed, macroscopic vortex-antivortex velocities, which in the creep regime are strongly temperature dependent:

$$\text{mod}(\mathbf{v}_\pm) = v_\pm = v_{\pm FF} \exp\left(-\frac{U}{T}\right). \tag{4}$$

$$\mathbf{J} = \frac{c}{4\pi}\nabla \times \mathbf{B}, \qquad \mathbf{B} = \varphi_0(n_+ - n_-), \qquad \mathbf{v}_{\pm FF} = \frac{\mathbf{J} \times \varphi_0}{\eta c}.$$

Here, U is a temperature-dependent pinning potential, φ_0 is the unit flux, $\mathbf{J}$ is the electric current, and η is the viscosity of the vortices, which in an anisotropic system is a tensor with different in plane and across the plane tensor components $\eta_{\alpha\beta}$.

(It should be noted that our master (recombination) equations account numbers of the *topological charges* (vortex/antivortex cores). The number of the vortices and antivortices is changed when they meet each other at the distance of the order of the coherence length ξ, rather than the penetration length of the magnetic field λ. For example, the same equations describe vortex-antivortex annihilation both in the superfluid He-4 and in superconducting films where the magnetic field is uniform).

We wish to investigate an anisotropic system where the vortices velocity is not necessarily parallel or perpendicular to the layers of the superconductor. Therefore, we shall take the vortices velocity in a general form

$$v_\alpha = -\gamma_{\alpha\beta}\left(\frac{\partial B}{\partial x_\beta}\right). \tag{5}$$

$\alpha, \beta = x, y.$

Here $\gamma = \varphi_0/4\pi\eta$ when

$$\gamma = \eta^{-1} = \eta_0^{-1}\begin{pmatrix} \cos^2\vartheta + \alpha\sin^2\vartheta & \cos\vartheta\sin\vartheta\,(1-\alpha) \\ \cos\vartheta\sin\vartheta\,(1-\alpha) & \alpha\cos^2\vartheta + \sin^2\vartheta \end{pmatrix} \tag{6}$$

is the inverse tensor of the vortex viscosity [20], α is the anisotropy parameter of the system ($0 < \alpha < 1$), ϑ is the angle between the x axis and the a–b plain of the layered structure (Fig. 1a).

Assuming that the heat flow from the thick film is running out in z-direction (the cold substrate is located in the plane $Z = 0$ (Fig. 1b)) one can complete the set of equations (1) and (2) by the temperature transfer equation in the form

$$C_p\frac{\partial T}{\partial t} = \kappa_T\,\nabla_{x,y}^2\,T + \frac{\delta Q}{\delta t} + \kappa_T\,\nabla_z^2\,T, \tag{7}$$

completed by the Newton boundary condition at the cooled substrate [27]:

$$\kappa_T[\nabla_z T]_{z=0} = -h(T - T_0); \tag{8}$$

$$[\nabla_z T]_{S\neq z=0} = 0. \tag{9}$$

Here

$$\frac{\partial Q}{\partial t} = W_J + W_A, \tag{10}$$

$$W_J = \frac{\eta v^2}{2}(n_+ + n_-); \qquad W_A = \xi v\frac{n_+ n_-}{C_p}Q_0 \tag{11}$$

is determined by the energy released both by vortex-antivortex dynamics W_J and by vortex-antivortex annihilation W_A. Here κ_T is the heat conductivity, C_p is the heat capacity, T_0 is the coolant temperature, Q_0 is heat released by annihilation of a single

vortex-antivortex pair per unit vortex length, h is the heat transfer coefficient to the coolant held at the temperature T_0.

Throughout this paper we consider current-carrying conditions whose transverse dimensions are sufficiently small (films). In this case (due to homogeneity in the z-direction) the last term in the (7) can be simplified [28]. Considering it as a sink term balancing heat term in a steady state and integrating both of them on volume of the sample one obtains (Fig. 1b):

$$\int dV \frac{\delta Q}{\delta t} = dDL \frac{\delta Q}{\delta t}$$

$$= \kappa_T \int dV \, \nabla_z^2 T = \kappa_T \oint_{Z=0} [\nabla_z T] dS = -h(T - T_0) dL, \quad (12)$$

where

$$\frac{\delta Q}{\delta t} = -\frac{h(T - T_0)}{d} \quad (13)$$

in equilibrium.

In non equilibrium the temperature transfer (7) reads:

$$C_p \frac{\partial T}{\partial t} = \kappa_T \, \nabla_{x,y}^2 T + \frac{\delta Q}{\delta t} - \frac{h(T - T_0)}{d}, \quad (14)$$

The set of (1)–(3) and (14) completed by the boundary conditions describes all features of the model. Here $t_R = C_p d / h$ is in the time units.

3 Spatial Distribution of Flux-antiflux Densities

We consider the case of a restricted sample of length D. In this case, the flux-antiflux interface in the stationary state is formed due to a balance between flux-antiflux entering the sample from the opposite sides and their annihilation in the middle point.

Introducing new variables

$$n_+/n_m = N_+, \qquad n_-/n_m = N_-, \qquad x/\Delta L \to x,$$

$$\Delta L = (n_m \xi)^{-1}, \qquad t/t_0 = t^*, \quad t_0 = \frac{\eta (\Delta L)^2}{n_m \varphi_0^2}, \quad (15)$$

$$b = N_+ - N_-, \qquad N = N_+ + N_-, \quad (16)$$

where n_m is flux density at the interface point, and ΔL is the characteristic width of the region in which the spatial distributions of vortex and antivortex flux densities overlap, forming the interlayer where the vortices of the opposite signs coexist. ΔL may be estimated as $\Delta L \simeq v/g n_m \sim (n_m \xi)^{-1}$ (see Ref. [29, 30]), which is a microscopically large area where the total magnetic induction is suppressed.

One obtain from (1)–(2)

$$\frac{\partial b}{\partial t^*} = \frac{\partial}{\partial x}\left(N\frac{\partial b}{\partial x}\right), \tag{17}$$

$$\frac{\partial N}{\partial t^*} = \frac{\partial}{\partial x}\left(b\frac{\partial b}{\partial x}\right) - |N^2 - b^2|\left|\frac{\partial b}{\partial x}\right|, \tag{18}$$

where b is the dimensionless magnetic induction.

In the stationary state we get for N_0 and b_0

$$\frac{\partial}{\partial x}\left(N_0\frac{\partial b_0}{\partial x}\right) = 0 \tag{19}$$

$$\frac{\partial}{\partial x}\left(b_0\frac{\partial b_0}{\partial x}\right) - (N_0^2 - b_0^2)\left|\frac{\partial b_0}{\partial x}\right| = 0. \tag{20}$$

Performing the integration in (19) one obtain

$$N_0\frac{\partial b_0}{\partial x} = -I. \tag{21}$$

here I is a constant.

Substituting N from (21) into (20) and performing the integration we immediately obtain the differential equation for b in the form

$$-W + \frac{I}{2}\ln\left|\frac{I+W}{I-W}\right| = -\frac{b_0^3}{3}. \tag{22}$$

where

$$W = b_0\frac{\partial b_0}{\partial x}. \tag{23}$$

3.1 Flux-Antiflux Interface

This equation may be solved analytically close to the interface line where b_0 goes to zero.

Assuming that the vortices and antivortices appear at the edges of the samples separated by the distance D (in dimensionless units) and assuming the following boundary conditions

$$b_0\frac{\partial b_0}{\partial x} = -I, \qquad N_{0-} = 0 \quad \text{at } x = -\frac{D}{2},$$

$$b_0\frac{\partial b_0}{\partial x} = I, \qquad N_{0+} = 0 \quad \text{at } x = \frac{D}{2}, \tag{24}$$

we obtain an asymptotically exact result for magnetic induction and vortices density at the interface: Looking for the solution in the vicinity of the flux-antiflux front

Fig. 2 Structure of the
vortex-antivortex interface
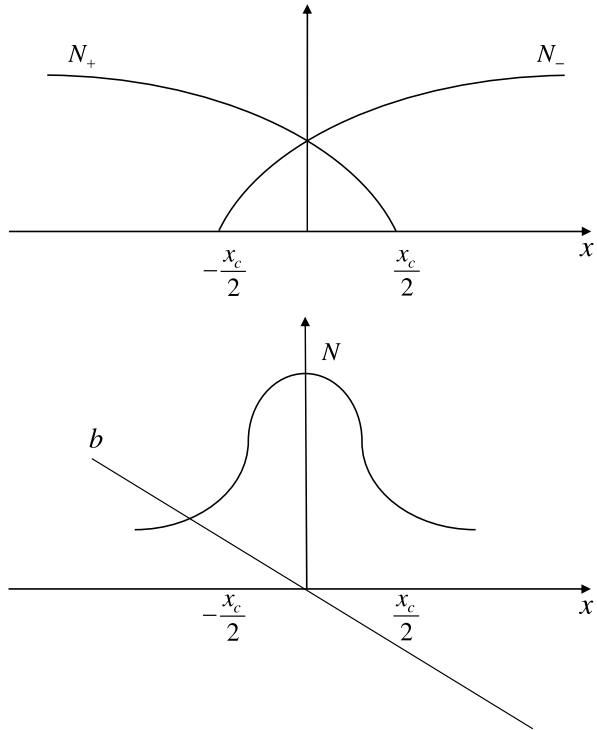
$(X \to 0)$ in the form

$$b_0 \simeq a_1 x + a_2 x^3; \qquad N_0 \simeq a_3 + a_4 x^2 \tag{25}$$

one obtains from (21), (23) to the main order

$$a_1 = -I^{2/3}, \qquad a_2 = \frac{I^{4/3}}{180}, \qquad a_3 = I^{1/3}, \qquad a_4 = \frac{I}{60}. \tag{26}$$

It should be noted numerical simulation show that these formulas are valid in a much wider region at front ($b_0 = 0$) and can be considered as an interpolation ones.

Assuming that the slope of the magnetic induction at the front $I \ll 1$ is small one obtains for the characteristic size of the vortex-antivortex area x_c, where vortices and antivortices coexist $N_0(x_c) = b_0(x_c)$ (see (19)) (see Fig. 2).

$$x_c = I^{-1/3} \gg 1. \tag{27}$$

The dimensionless vortex velocity at the interface $u_0 = I^{2/3}$ is a constant. Returning to the dimension variables, we obtain for interface flux velocity

$$u_\pm \approx \frac{n_m^2 \xi \varphi_0^2}{4\pi} \frac{\exp(-U/T)}{\eta} I^{2/3}. \tag{28}$$

4 Overheating Instability

Let us consider the stability of the vortex-antivortex interface with respect to small deviations from its initial plane shape. For this we shall take the (14), (17) and (18), in the more general form

$$\frac{\partial b}{\partial t} - \nabla(N\mathbf{v}) = 0, \tag{29}$$

$$\frac{\partial N}{\partial t} - \nabla(b\mathbf{v}) + (N^2 - b^2)|v| = 0, \tag{30}$$

$$\frac{\partial \Theta}{\partial t} - \kappa \nabla^2 \Theta - w_A - w_J + r(\Theta - 1) = 0, \tag{31}$$

where

$$w_A = (N^2 - b^2)S_A|v|, \qquad w_J = NS_J v^2 \tag{32}$$

are the dimensionless annihilation and Joule heat terms. Here $S_A \equiv (Q_0 n_m/4\pi T_0 C_p)$; $S_J = \varphi_0^2 n_m^2/16\pi^2 T_0 C_p$ are the heating parameters, $Q_0 \sim \varphi_0^2/\lambda^2$ where λ is the London penetration length. The ratio $S_J/S_A \sim \lambda^2 n_m$.

It seems at first glance that the direct Joule term caused by vortex (antivortex) motion always prevails. Really, for a sharp shape magnetic induction front the vortex-antivortex annihilation term (overlapping) which is proportional to the vortex (antivortex) density production $w_A \sim vN_+N_-$ is small while vortex velocity $v \sim \nabla b$ is large. Therefore the direct, Joule term which is proportional both to the sum of the vortex and antivortex densities and to the square of the velocity $w_J = NS_J v^2$ significantly exceeds the annihilation term. *However, in our case, when the slope of the magnetic induction profile is small the annihilation term becomes essentially important.* In this case the overlapping (annihilation) term is larger due to deep mutual penetration of vortices and antivortices over the interface area (see Fig. 2). The vortex velocity in this case is small and it decreases the Joule term which is of the order of v^2. Substituting functions N_+, N_- from the (25), (26), (16) into (32) one obtains for the $w_J \simeq N_0(\nabla b_0)^2 \simeq I^{5/3}$ and $w_A \sim N_0^2 \nabla b_0 \simeq I^{4/3}$ allowing to neglect in our consideration the Joule term which is relatively small

$$w_J/w_A \simeq I^{1/3} \ll 1. \tag{33}$$

Here the dimensionless velocity v has the form

$$v = \exp(-U/T)\left|\frac{\partial b}{\partial x}\right| \tag{34}$$

while $\kappa \to t_0 \kappa_T/c_p(\Delta L)^2$ (here $\kappa_d = \kappa_T/C_p$ is the diffusion constant), $r \to t_0/t_R$ are the dimensionless effective diffusion and relaxation coefficients correspondingly.

4.1 Small Fluctuations

Looking for a solution of the form

$$b(x, y, t) = b_0(x) + \psi(x, y, t), \tag{35}$$

$$N(x, y, t) = N_0 + \zeta(x, y, t), \tag{36}$$

$$\Theta(x, y, t) = 1 + \theta(x, y, t), \tag{37}$$

where ψ, ζ and θ are the small perturbations of the form

$$\begin{pmatrix} \psi(x, y, t) \\ \zeta(x, y, t) \\ \theta(x, y, t) \end{pmatrix} = \begin{pmatrix} \psi(x) \\ \zeta(x) \\ \theta(x) \end{pmatrix} \exp(\lambda_r t + iky). \tag{38}$$

Here ψ_0, ζ_0 and θ_0 are constant amplitudes, λ_r is the rate grow of the perturbation and k is the wave vector in the y direction.

Taking into account the fluctuations of the vortex velocity

$$v_\alpha = -(1 + \theta)\gamma_{\alpha\beta} \frac{\partial b}{\partial x_\beta}, \tag{39}$$

where θ/T_0 is the change of velocity due to thermal fluctuations [29, 30] and $\gamma = \varphi_0/4\pi\eta$ (see (6)) one obtains

$$
\begin{aligned}
v_x &= v_x^0 + \delta v_x = -\gamma_{xx}\frac{\partial b_0}{\partial x} - \gamma_{xx}\frac{\partial \psi}{\partial x} - \gamma_{xx}\frac{\partial b_0}{\partial x}\theta - \gamma_{xy}\frac{\partial \psi}{\partial y}, \\
v_y &= v_y^0 + \delta v_y = -\gamma_{yx}\frac{\partial b_0}{\partial x} - \gamma_{yx}\frac{\partial \psi}{\partial x} - \gamma_{yx}\frac{\partial b_0}{\partial x}\theta - \gamma_{yy}\frac{\partial \psi}{\partial y}.
\end{aligned}
\tag{40}
$$

Here $\delta v_{x,y}$ are the deviations from the steady state vortex velocity.

While the vortex velocity in the x direction is higher then in the y direction, we assume that $|v| \approx v_x$.

We neglect the influence of temperature fluctuations on heat capacity C_p and relaxation coefficient r because their calculations do not result in essential effects. We also neglect in the main order the change of the average temperature in the flux front area.

Substituting the perturbations in the form (38) into initial set of (29)–(31), and use the stationary solution in the form (19)–(20) (see Appendix 2) one obtains from the (72) for the rate grow

$$\lambda_r^3 + \lambda_r^2(\Gamma_1 + \Pi_1 k^2) + \lambda_r(\Gamma_2 + \Pi_2 k^2 + \Pi_3 k^4) + (\Pi_4 k^2 + \Pi_5 k^4) = 0, \tag{41}$$

where $\gamma_{xy} = \gamma_{yx}$ and

$$\Gamma_1 = 2\gamma_{xx}I + r - \gamma_{xx}I^{\frac{4}{3}}S_A, \tag{42}$$

Fig. 3 (Color online)
Mullins-Sekerka instability for
super large heat. The increment
Re λ versus k^2 (k is the wave
vector along the flux-antiflux
front)
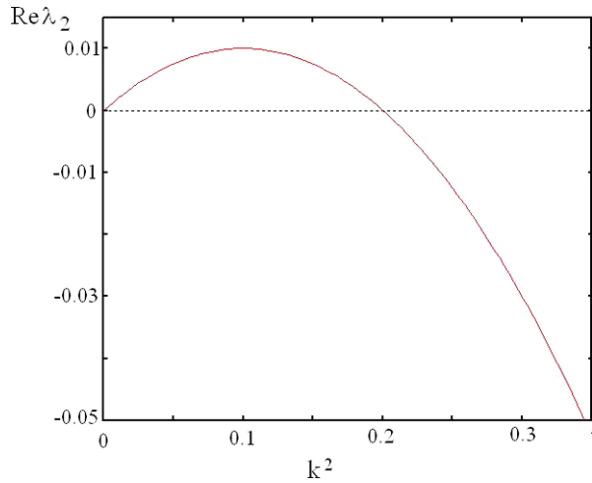
$$\Pi_1 = -\gamma_{yy} I^{\frac{1}{3}} + \kappa,$$

$$\Gamma_2 = 2\gamma_{xx} I r,$$

$$\Pi_2 = 2(\gamma_{xy}^2 - \gamma_{xx}\gamma_{yy}) I^{\frac{4}{3}} + 2\gamma_{xx} I \kappa - \gamma_{yy} I^{\frac{1}{3}} r + I^{\frac{5}{3}} S_A (\gamma_{xx}\gamma_{yy} - \gamma_{xy}^2),$$

$$\Pi_3 = -\gamma_{yy} I^{\frac{1}{3}} \kappa,$$

$$\Pi_4 = 2(\gamma_{xy}^2 - \gamma_{xx}\gamma_{yy}) r I^{\frac{4}{3}} + \gamma_{xx}\gamma_{xy}^2 S_A I^{\frac{8}{3}},$$

$$\Pi_5 = 2(\gamma_{xy}^2 - \gamma_{xx}\gamma_{yy}) \kappa I^{\frac{4}{3}}.$$

The roots of these equations are presented in Appendix 2 where the solution $\lambda_{1,2}$
are relevant.

(We consider only the nonuniform instability, hence solutions with Re $\lambda > 0$ at $k = 0$ are omitted). The onset of the nonuniform along the front instability is determined
either by the conditions (Re $\lambda_1 = 0$)

$$(\text{Re } B_1)^2 = 4(\text{Re } C_1)(\text{Re } A_1), \qquad (43)$$

$$\text{Re } C_1 < 0, \qquad (\text{Re } A_1) < 0 \qquad (44)$$

giving the contact point at Re $\lambda_1 - k^2$ plane (see Figs. 3–5)

$$k^2 = -\frac{\text{Re } B_1}{2 \text{ Re } A_1} \qquad (45)$$

or at $C_1 = 0$ (Re $B_1 > 0$, Re $A_1 < 0$) resulting in the Mullins-Sekerka instability.

Fig. 4 (Color online) The increment $\mathrm{Re}\,\lambda$ versus k^2 for isotropic superconductors ($\alpha = 0.9$, $\vartheta = \pi/4$) with different in-plane diffusion constant κ. Curves 1, 2, 3 correspond to $\kappa = 0.1; 0.5; 1$ respectively. Here $\gamma_{xx} = \gamma_{yy} = 0.545$, $\gamma_{xy} = 0.055$, $I = 0.5$, $r = 0.0148$, $S_A = 0.89$. Instability disappears as the diffusion constant grows
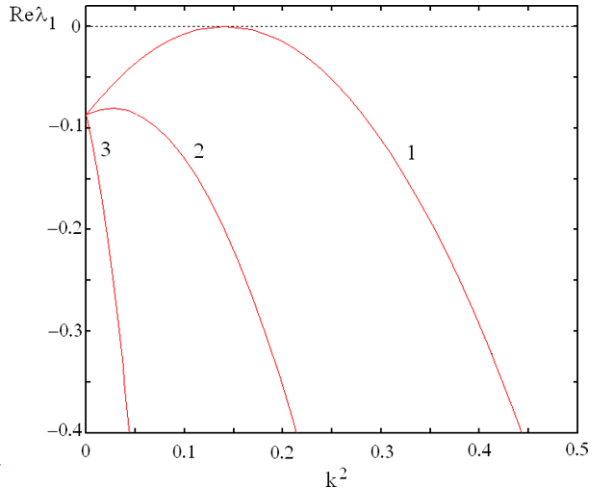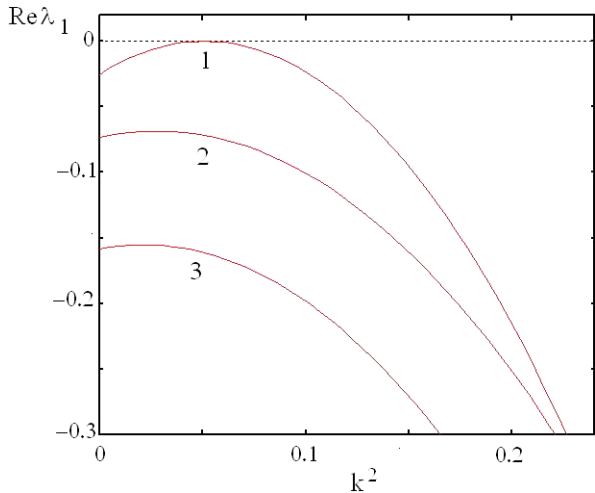

Fig. 5 (Color online) The increment $\mathrm{Re}\,\lambda$ versus k^2 for anisotropic superconductor with different relaxation constant r. Curves 1, 2, 3 correspond to parameters $r = 0.049; 0.13; 2.66$ respectively. The instability disappears as the relaxation parameter grows. Here $\gamma_{xx} = \gamma_{yy} = 0.545$, $\gamma_{xy} = 0.055$, $\kappa = 0.1$, $I = 0.5$, $S_A = 0.89$

5 Results

5.1 Strong Heating

We start with a model case when the heating coefficient $S \to \infty$. In this case the parameters of the dispersion (42) have the form

$$\Gamma_1 = -\gamma_{xx} I^{\frac{4}{3}} S_A; \qquad \Pi_1 = -\gamma_{yy} I^{\frac{1}{3}} + \kappa; \qquad \Gamma_2 = 2\gamma_{xx} I r;$$

$$\Pi_2 = I^{\frac{5}{3}} S_A (\gamma_{xx}\gamma_{yy} - \gamma_{xy}^2);$$

$$\Pi_3 = -\gamma_{yy} I^{\frac{1}{3}} \kappa; \qquad \Pi_4 = \gamma_{xx}\gamma_{xy}^2 S_A I^{\frac{8}{3}}; \qquad \Pi_5 = 2(\gamma_{xy}^2 - \gamma_{xx}\gamma_{yy})\kappa I^{\frac{4}{3}};$$

$$\tag{46}$$

$$\sqrt{\Gamma_1^2 - 4\Gamma_2} = \gamma_{xx} I^{4/3} S_A$$

while the equation for $\operatorname{Re}\lambda_2$ function reads (see Appendix 2)

$$\operatorname{Re}\lambda_2 = \frac{\gamma_{xy}^2 S_A I^{\frac{5}{3}}}{4r} k^2 - \frac{\gamma_{xy}^4 S_A^3 I^{\frac{11}{3}}}{64 r^3} k^4. \tag{47}$$

The rapidly growing mode in this case $d^2 \operatorname{Re}\lambda_2/dk^2 = 0$ (maximum velocity of the mostly unstable mode) has the wave vector $k = 2\sqrt{2}r/\sqrt{3}\gamma_{xy} S_A I$ and the period of the pattern along the front (see Fig. 3)

$$d_y = \sqrt{\frac{3}{2}} \frac{\pi \gamma_{xy} S_A I}{r}. \tag{48}$$

In the case of moderate and small heating parameter S_A, the results are strongly depends both on anisotropy and on the relation between other parameters and can be done numerically.

5.2 Moderate and Weak Heating

In this case the equation for real part of the increment of the instability is determined by the equation (see Appendix 3)

$$\operatorname{Re}\lambda_1 = \operatorname{Re} C_1 + k^2 \operatorname{Re} B_1 + k^4 \operatorname{Re} A_1. \tag{49}$$

It has been solved for different anisotropy, in-plane diffusion coefficients κ and relaxation coefficients r. The results are presented in Figs. 4–6. In all of the curves at these figures the $\operatorname{Re} C_1 < 0$, $\operatorname{Re} B_1 > 0$ and $\operatorname{Re} A_1 < 0$.

The instabilities in all of these cases has the form of contact one rather than the Mullins-Sekerka type. The nonuniform structure along the front appears with the period $d_y = 2\pi/k_c$ where k_c is the contact point of the $\operatorname{Re}\lambda_1$ with k axis.

In Fig. 4 the $\operatorname{Re}\lambda_1$ as a function of k^2 is shown for anisotropic superconductors with various in-plane diffusion constant κ. There is a critical heating parameter S and critical diffusion constant when the instability arises (curve 1), while the system becomes stable as the diffusion constants increase (curve 2,3). The relaxation constant r (the coefficient of the ballistic heat conductivity) also strongly affect the instability condition. In Fig. 5 the increment $\operatorname{Re}\lambda$ versus k^2 for anisotropic superconductor with different relaxation constant r demonstrate that the instability appearing at relatively small constant r (see curve 1) disappears as the relaxation parameter grow (curves 2, 3).

Figure 6 demonstrates that the anisotropy essentially affects the onset of the instability. The increment of instability $\operatorname{Re}\lambda$ versus k^2 for different anisotropy. Curve 1 for isotropic superconductor ($\alpha = 0.9$, $\vartheta = \pi/4$, $\gamma_{xx} = \gamma_{yy} = 0.545$, $\gamma_{xy} = 0.055$) shows the instability at heating coefficient $S_A = 0.89$ while curve 2 demonstrates the lack of instability at heating coefficient $S_A = 0.8$. The curve 3 exhibits instability for anisotropic superconductor ($\alpha = 0.1$, $\vartheta = \pi/4$, $\gamma_{xx} = \gamma_{yy} = 0.55$, $\gamma_{xy} = 0.45$) and even more small heating coefficient $S_A = 0.1$.

Fig. 6 (Color online) The increment of instability $\mathrm{Re}\,\lambda$ versus k^2 for different anisotropy. Curve 1 for isotropic superconductor ($\alpha = 0.9$, $\vartheta = \pi/4$, $\gamma_{xx} = \gamma_{yy} = 0.545$, $\gamma_{xy} = 0.055$) shows the instability at heating coefficient $S_A = 0.89$ while curve 2 demonstrates the lack of instability at heating coefficient $S_A = 0.8$. The curve 3 exhibits instability for anisotropic superconductor ($\alpha = 0.1$, $\vartheta = \pi/4$, $\gamma_{xx} = \gamma_{yy} = 0.55$, $\gamma_{xy} = 0.45$) and even more small heating coefficient $S_A = 0.1$. (Here $r = 0.0148$, $\kappa = 0.1$, $I = 0.5$.)
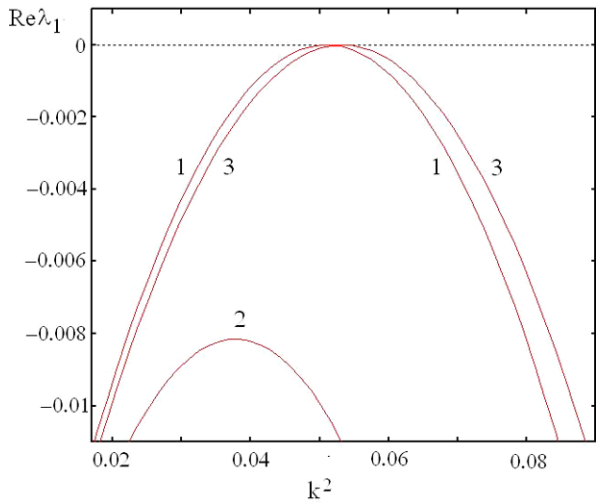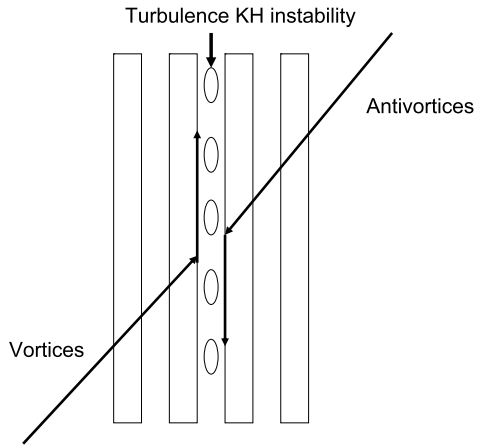

Fig. 7 Qualitative picture of the Kelvin-Helmholtz instability at the vortex-antivortex interface

6 Conclusions

We considered the flux-antiflux instability in a thick film subjected to the oppositely directed magnetic field H (z-direction) at the sample edges. The field creates vortices and antivortices penetrating the sample and annihilating in the center of the film (Fig. 1b). Electromagnetically the film is not thin in the Pearl sense, (namely the thickness in our case does not obey $d \ll \lambda$), so the relation between the current density and the magnetic induction is local. We found that the standing flux-antiflux interface where vortices and antivortices coexist (Meissner hole) demonstrates instability due to the heat released by the flux-antiflux annihilation. In fact this is a well known Kelvin-Helmholtz (KH) instability appearing when different layers of liquid move with the opposite directed velocities [19]. In our case, however, vortex and antivortex "liquids" are moving as it is shown in Fig. 7. The heat released by the annihilation enhances the vortex/antivortex velocities ("tornado effect") resulting in

turbulence instability at the flux-antiflux interface. The rate grow dependence on the wave vector directed along the front showing the instability is presented in Figs. 3–6 for different heating parameters and anisotropy of the superconducting materials. The characteristic size of the unstable pattern is determined either by the rapidly growing mode of the real part of the rate grow $d\lambda_2/dk$ (for strong heating parameter) (see Fig. 3) or at the contact mode for moderate and small heating (Figs. 4–6).

The theory predicts stability of the flux-antiflux front for any physical parameter of the system (see (73) from Appendix 3). The physical reason for the instability is the result of growing temperature gradients along the front when vortices are moving with different velocities. The velocity of the flux flow vortices is very high and more rapid parts of the front can break it during the time of the instability. In particular for materials with typical parameters

$$B = 1000 \text{ G}, \qquad \eta = 5 \times 10^{-5} \text{ CGSE}, \qquad v_F = 10^7 \text{ cm/s},$$
$$l = 10^{-8} \text{ cm}, \qquad \xi = 10^{-6} \text{ cm}, \tag{50}$$

where B, η, v_F, l are the magnetic induction, viscosity, Fermi velocity and mean path length of the electron correspondingly, $n_m = B/\phi_0 \sim 10^{10}$ cm^{-2} one obtains for characteristics units of time, space and diffusion constant κ_d (see (15))

$$t_0 \simeq 5 \times 10^{-8} \text{ s}, \qquad \Delta L \simeq 10^{-4} \text{ cm}, \qquad \kappa_d = \frac{(\Delta L)^2}{t_0}\kappa \simeq \kappa \tag{51}$$

the characteristic size of the interface in the dimension units $L_c \simeq \Delta L/I^{1/3}$ (Meissner hole).

For BCS superconductor where $\Delta \to 0$ the dimensional heating parameter $S_A \simeq n_m v_F^2/T_0^2 \simeq \xi^2 n_m < 1$ (here $C_p \simeq m p_F T$, while ε_F and p_F are the Fermi energy and the momentum correspondingly. At low temperature $T < \Delta_0$, where $C_p \simeq (m p_F \Delta_0^{5/2}/T_0^{3/2}) \exp(-\Delta_0/T)$ the heating parameter S_A grows dramatically $S_A \simeq \frac{n_m v_F^2}{\Delta_0^2}(\frac{T_0}{\Delta_0})^{1/2} \exp(\Delta_0/T) \gg 1$.

The heat parameter S_A is responsible for type of the instability. In particular at low temperatures ($T_0 \ll T_c$, where T_c is the critical temperature) the parameter S_A is large and the instability develops on Mullins-Sekerka scenario (see Fig. 3) typical for dendritic instability [4]. On the other hand, at temperatures close to the critical, when the heating parameter $S_A < 1$, the instability emerges as a periodic pattern (see Figs. 4–6) [31].

Vortices and antivortices in the unstable pattern move with velocities (see (28)) $u \simeq 10^5$ cm/s. If the difference of the "rapid" and "slow parts" of the front $\delta v \sim 10u$ the flux pattern might reach the microscopic magnitudes L for very short time of the instability development $\tau \simeq 30$ μs, $L \approx 3$ cm. The heat fluctuation for this time cannot significantly relaxes because it moves along the front on distance $\delta y \simeq \sqrt{\kappa\tau} \sim 0.01$ cm.

The main results of this paper are presented in Figs. 3–6 where the increments of the instability were drown for various anisotropy parameter α, heat conductivities inside and across the sample (κ and r correspondingly) and heat annihilation coefficient S_A. We conclude that heat released by the flux-antiflux annihilation results in

instability of the interface separating fluxons and antifluxons areas even in the case of weak anisotropy of the superconductor.

On the other hand if the superconductor is strongly anisotropic, the instability emerges even for weak heat. In more experimentally common case of moderated heat and anisotropy, both these mechanisms work together creating the instability of the flux-antiflux front.

Our major conclusion is that the anisotropy of the superconducting layered structure alone cannot explain instability of the flux antiflux interface in weakly anisotropic materials as Nb and MgB_2. From this point of view without the heating, the flux-antiflux front in the Nb superconductor ($\alpha \simeq 0.9$) without heating should be stable for any angle ϑ while strong heating destroys the front. If the heating caused by the vortex-antivortex annihilation is large then the vortex antivortex front instability should be detected in completely isotropic superconductors like MgB_2 (Fig. 6, curve 1). In fact it should be noted that even small heating might be essentially important to cause the instability.

Resent results by Mohan et al. [21] shows that instability arises in optimally doped $Ba(Fe_{1-x}Co_x)_2As_2$ superconductor with small anisotropy. The small slope of the induction at the flux-antiflux front extracted from Fig. 3 of the manuscript ($db/dx = I^{2/3} = 0.2$ in dimensionless units) demonstrate vortex-antivortex mechanism of the turbulence in this material (see (33)).

This theory is appropriate in the flux flow regime. The spatial disorder might affect the result by two different ways. It can both modify the linear profile of the magnetic induction at the front and affect the mechanism of the heat at the interface.

Appendix 1

Considering vortices (antivortices) as particles with coordinates $r_i(t)$ and the microscopic vortex (antivortex) density in the form

$$n_{\pm}^M(r, t) = \sum_{i=1}^{N} \delta(r - \mathbf{r}_i(t)), \qquad (52)$$

one obtains

$$\frac{\partial n_{\pm}^M}{\partial t} = \sum_{i=1}^{N} \frac{\partial \delta(\mathbf{r} - \mathbf{r}_i)}{\partial r_i} \mathbf{v}_i^M, \qquad (53a)$$

where the microscopic vortex (antivortex) velocity

$$\mathbf{v}_i^M = \frac{d\mathbf{r}_i}{dt} = \mathbf{F}_i^M / \eta. \qquad (54)$$

Here the force field $\mathbf{F}_i(r, t)$ can be presented in the form

$$\mathbf{F}_i^M = \frac{\mathbf{J}_i^M \times \mathbf{z}\varphi_0}{c}, \qquad (55)$$

where $\mathbf{J}_i^M$ is the microscopic current density consisting of both the external current and of the local current density caused by the interaction of the i-th vortex with the entire vortex system. Using the properties of the δ-function

$$\frac{\partial}{\partial \mathbf{r}_i}\delta(\mathbf{r}-\mathbf{r}_i(t)) = -\frac{\partial}{\partial \mathbf{r}}\delta(\mathbf{r}-\mathbf{r}_i(t)),$$

$$\sum_{1<i<N} f(r_i)\delta(\mathbf{r}-\mathbf{r}_i) = f(r)\sum_{1<i<N}\delta(\mathbf{r}-\mathbf{r}_i) \qquad (56)$$

and averaging the microscopic equation over a small volume, one obtains the master equation for the vortex dynamics completed by the sink annihilation term in the form given by (1)–(3). In these equations the macroscopic velocity is defined by $\mathbf{v} = \overline{\mathbf{v}_i^M} = \overline{\mathbf{F}_i^M}/\eta = \overline{\mathbf{J}_i^M}\times\mathbf{z}\varphi_0/c\eta$, see (4), where $\mathbf{J} = \overline{\mathbf{J}_i^M}$ is the macroscopic current density.

In fact, however, the velocity in the sink term is microscopic velocity caused both by the external current and by vortex-antivortex attraction $\mathbf{v}^M = \mathbf{v} + \mathbf{v}_{int}$, where

$$\mathbf{v}_{int} = \mathbf{F}_{int}^M/\eta \simeq \left(\frac{\varphi_0}{4\pi\lambda}\right)^2\frac{1}{\eta a_0} \qquad (57)$$

and a_0 is the mean intervortex distance, λ is the London penetration length.

The ratio

$$\frac{v_{int}}{v} \simeq \frac{a_0^3}{4\pi\lambda^2\xi I^{2/3}} \ll 1 \qquad (58)$$

is assumed to be small.

Here the hydrodynamics velocity is estimated as $v \simeq J\varphi_0/c\eta \simeq \nabla B\varphi_0/4\pi\eta \simeq I^{2/3}n_0^2\xi\varphi_0^2/4\pi\eta$, where we used the relations (see (15), (25))

$$B = n_m\varphi_0 b, \qquad \nabla B \simeq \frac{n_m\varphi_0\partial b}{\Delta L\partial x} \sim \frac{n_m\varphi_0}{\Delta L}I^{2/3} \qquad (59)$$

and $a_0 \simeq n_m^{-1/2}$. Hence, in this approximation, the microscopic velocity in the sink term can be replaced by the averaged, hydrodynamic velocity v in the basic (1)–(3).

Appendix 2

Substituting (35)–(40) in the initial set of (29)–(31), and use the stationary solution in the form (19)–(20) one obtains for perturbations

$$\frac{\partial\psi}{\partial t} - N_0\frac{\partial\delta v_x}{\partial x} - \zeta\frac{\partial v_x^0}{\partial x} - v_x^0\frac{\partial\zeta}{\partial x} - N_0\frac{\partial\delta v_y}{\partial y} - v_y^0\frac{\partial\zeta}{\partial y} = 0, \qquad (60)$$

$$\frac{\partial\zeta}{\partial t} - \frac{\partial b_0}{\partial x}\delta v_x - b_0\frac{\partial\delta v_x}{\partial x} - v_x^0\frac{\partial\psi}{\partial x} - b_0\frac{\partial\delta v_y}{\partial y} - v_y^0\frac{\partial\psi}{\partial y} + 2(N_0\zeta - b_0\psi)v_x^0, \qquad (61)$$

$$\frac{\partial \theta}{\partial t} - \kappa\left(\frac{\partial^2 \theta}{\partial x^2} + \frac{\partial^2 \theta}{\partial y^2}\right) - 2S_A(N_0\zeta - b_0\psi)v_x^0 + r\theta = 0. \qquad (62)$$

Looking for the solution of these equations in the form (38) one obtains near the interface where $b_0 = -I^{2/3}x$, $N_0 = I^{1/3}$ (see (25), (26)) the set of differential equations with uniform coefficients:

$$(\lambda - \gamma_{yy}I^{\frac{1}{3}}k^2)\psi(x) + (\gamma_{xy} + \gamma_{yx})ikI^{\frac{1}{3}}\frac{\partial\psi(x)}{\partial x} + \gamma_{xx}I^{\frac{1}{3}}\frac{\partial^2\psi(x)}{\partial x^2} - \gamma_{yx}ikI^{\frac{2}{3}}\zeta(x),$$

$$- \gamma_{xx}I^{\frac{2}{3}}\frac{\partial\zeta(x)}{\partial x} - \gamma_{yx}ikI\theta(x) - \gamma_{xx}I\frac{\partial\theta(x)}{\partial x} = 0, \qquad (63)$$

$$-2\gamma_{xy}ikI^{\frac{2}{3}}\psi(x) - 2\gamma_{xx}I^{\frac{2}{3}}\frac{\partial\psi(x)}{\partial x} + (\lambda + 2\gamma_{xx}I)\zeta(x) + \gamma_{xx}I^{\frac{4}{3}}\theta(x) = 0, \quad (64)$$

$$\gamma_{xy}ikI^{\frac{2}{3}}S_A\psi(x) + \gamma_{xx}I^{\frac{2}{3}}S_A\frac{\partial\psi(x)}{\partial x} - 2\gamma_{xx}IS_A\zeta(x)$$

$$+ (\lambda + r + \kappa k^2 - \gamma_{xx}I^{\frac{4}{3}}S_A)\theta(x) - \kappa\frac{\partial^2\theta(x)}{\partial x^2} = 0. \qquad (65)$$

These equations should be completed by the boundary conditions

$$\begin{pmatrix} \psi \\ \zeta \\ \theta \end{pmatrix}_{x=-x_c/2, x_c/2} = 0. \qquad (66)$$

The functions $\psi(x)$, $\zeta(x)$ and $\theta(x)$ should be symmetrical and localized at the flux-antiflux interface where $x < x_c$ while $x_c \gg 1$ is the cutoff where these functions go to zero (see Fig. 2 and (27)).

Looking for solution of (60)–(65) in the form

$$\begin{pmatrix} \psi \\ \zeta \\ \theta \end{pmatrix} = \begin{pmatrix} (A_n \sin p_n x + B_n \cos p_n x) \\ (C_n \sin p_n x + D_n \cos p_n x) \\ (E_n \sin p_n x + F_n \cos p_n x) \end{pmatrix}; \qquad (67)$$

one obtains equations for $A_n, B_n, C_n, D_n, E_n, F_n$ coefficients

$$\widehat{\Lambda} \begin{pmatrix} A_n \\ B_n \\ C_n \\ D_n \\ E_n \\ F_n \end{pmatrix} = 0, \qquad (68)$$

where matrix $\widehat{\Lambda}$ reads

$$
\begin{pmatrix}
\lambda_r - \gamma_{yy}I^{\frac{1}{3}}k^2 - & -2\gamma_{xy}ip_nkI^{\frac{1}{3}} & -\gamma_{yx}ikI^{\frac{2}{3}} & p_n\gamma_{xx}I^{\frac{2}{3}} & -\gamma_{yx}ikI & p_n\gamma_{xx}I \\
-\gamma_{xx}I^{\frac{1}{3}}p_n^2 & & & & & \\
p_n2\gamma_{xy}ikI^{\frac{1}{3}} & \lambda_r - \gamma_{yy}I^{\frac{1}{3}}k^2 - & -\gamma_{xx}I^{\frac{2}{3}}p_n & -\gamma_{yx}ikI^{\frac{2}{3}} & -\gamma_{xx}Ip_n & -\gamma_{yx}ikI \\
 & -\gamma_{xx}I^{\frac{1}{3}}p_n^2 & & & & \\
-2\gamma_{xy}ikI^{\frac{2}{3}} & 2p_n\gamma_{xx}I^{\frac{2}{3}} & \lambda_r + 2\gamma_{xx}I & 0 & \gamma_{xx}I^{\frac{4}{3}} & 0 \\
-2p_n\gamma_{xx}I^{\frac{2}{3}} & -2\gamma_{xy}ikI^{\frac{2}{3}} & 0 & \lambda_r + 2\gamma_{xx}I & 0 & \gamma_{xx}I^{\frac{4}{3}} \\
\gamma_{xy}ikI^{\frac{2}{3}}S_A & -\gamma_{xx}I^{\frac{2}{3}}SP_n & -2\gamma_{xx}IS_A & 0 & \lambda_r + r + \kappa k^2 - & 0 \\
 & & & & -\gamma_{xx}I^{\frac{4}{3}}S_A + \kappa p_n^2 & \\
\gamma_{xx}I^{\frac{2}{3}}S_A P_n & \gamma_{xy}ikI^{\frac{2}{3}}S_A & 0 & -2\gamma_{xx}IS_A & 0 & \lambda_r + r + \kappa k^2 - \\
 & & & & & -\gamma_{xx}I^{\frac{4}{3}}S_A + \kappa p_n^2
\end{pmatrix}
\tag{69}
$$

where $p_n = (2n + 1)\pi/x_c$ is obtained from the boundary condition (66). The dangerous harmonic with $n = 0$ is responsible for instability. In this case $p_0 \sim x_c^{-1} \sim I^{1/3} \to 0$ for small slope of the magnetic induction at the interface ($I \ll 1$) this matrix can be simplified:

$$
\begin{vmatrix}
\lambda - \gamma_{yy}I^{\frac{1}{3}}k^2 & 0 & & -\gamma_{yx}ikI^{\frac{2}{3}} & 0 \\
0 & \lambda - \gamma_{yy}I^{\frac{1}{3}}k^2 & 0 & -\gamma_{yx}ikI & 0 \\
-2\gamma_{xy}ikI^{\frac{2}{3}} & 0 & \lambda + 2\gamma_{xx}I & 0 & 0 & -\gamma_{yx}ikI \\
0 & -2\gamma_{xy}ikI^{\frac{2}{3}} & 0 & & \gamma_{xx}I^{\frac{4}{3}} & 0 \\
\gamma_{xy}ikI^{\frac{2}{3}}S_A & 0 & -2\gamma_{xx}IS_A & 0 & \lambda + r + \kappa k^2 - \gamma_{xx}I^{\frac{4}{3}}S_A & 0 \\
0 & \gamma_{xy}ikI^{\frac{2}{3}}S_A & 0 & -2\gamma_{xx}IS_A & 0 & \lambda + r + \kappa k^2 - \gamma_{xx}I^{\frac{4}{3}}S_A
\end{vmatrix} = 0,
\tag{70}
$$

and can be represented as generated Jordan matrix.

$$
\begin{vmatrix}
\widehat{K} & 0 \\
0 & \widehat{K}
\end{vmatrix} = 0,
\tag{71}
$$

where K is the 3×3 matrix

$$
\widehat{K} =
\begin{vmatrix}
(\lambda_r - \gamma_{yy}I^{\frac{1}{3}}k^2) & (-\gamma_{yx}ikI^{\frac{2}{3}}) & (-\gamma_{yx}ikI) \\
(-2\gamma_{xy}ikI^{\frac{2}{3}}) & (\lambda_r + 2\gamma_{xx}I) & (\gamma_{xx}I^{\frac{4}{3}}) \\
(\gamma_{xy}ikI^{\frac{2}{3}}S_A) & (-2\gamma_{xx}IS_A) & (\lambda_r + r + \kappa k^2 - \gamma_{xx}I^{\frac{4}{3}}S_A)
\end{vmatrix}
\tag{72}
$$

giving the equation for in the form (41)–(42).

Appendix 3

The solutions of the (41)–(42) at small $k \to 0$ read:

$$\lambda_0 = -\frac{\Pi_4}{\Gamma_2}k^2 + A_0 k^4; \tag{73}$$

$$A_0 = \frac{\Pi_2 \Pi_4}{\Gamma_2^2} - \frac{\Gamma_1 \Pi_4^2}{\Gamma_2^3} - \frac{\Pi_5}{\Gamma_2}; \tag{}$$

$$\lambda_1 = C_1 + B_1 k^2 + A_1 k^4; \tag{74}$$

$$C_1 = \frac{1}{2}\left[-\Gamma_1 + \sqrt{\Gamma_1^2 - 4\Gamma_2}\right]; \tag{75}$$

$$B_1 = \frac{[\Gamma_1 - \sqrt{\Gamma_1^2 - 4\Gamma_2}][\Gamma_1 \Pi_1 - \Pi_2] + 2[\Pi_4 - \Gamma_2 \Pi_1]}{\Gamma_1[\sqrt{\Gamma_1^2 - 4\Gamma_2} - \Gamma_1] + 4\Gamma_2}; \tag{76}$$

$$A_1 = \frac{B_1^2[3\sqrt{\Gamma_1^2 - 4\Gamma_2} - \Gamma_1] + [\sqrt{\Gamma_1^2 - 4\Gamma_2} - \Gamma_1][2B_1 \Pi_1 + \Pi_3] + 2[\Pi_5 + B_1 \Pi_1]}{4\Gamma_2 + \Gamma_1[\sqrt{\Gamma_1^2 - 4\Gamma_2} - \Gamma_1]}; \tag{77}$$

and

$$\lambda_2 = C_2 + B_2 k^2 + A_2 k^4; \tag{78}$$

$$C_2 = \frac{1}{2}\left[-\Gamma_1 - \sqrt{\Gamma_1^2 - 4\Gamma_2}\right]; \tag{}$$

$$B_2 = \frac{[\Gamma_1 + \sqrt{\Gamma_1^2 - 4\Gamma_2}][\Pi_2 - \Gamma_1 \Pi_1] + 2[\Gamma_2 \Pi_1 - \Pi_4]}{\Gamma_1[\sqrt{\Gamma_1^2 - 4\Gamma_2} + \Gamma_1] - 4\Gamma_2}; \tag{79}$$

$$A_2 = \frac{B_2^2[3\sqrt{\Gamma_1^2 - 4\Gamma_2} + \Gamma_1] + [\sqrt{\Gamma_1^2 - 4\Gamma_2} + \Gamma_1][2B_2 \Pi_1 + \Pi_3] - 2[\Pi_5 + B_2 \Pi_1]}{\Gamma_1[\sqrt{\Gamma_1^2 - 4\Gamma_2} + \Gamma_1] - 4\Gamma_2}. \tag{80}$$

References

1. V.K. Vlasko-Vlasov et al., Physica C **222**, 361 (1994)

2. M.R. Koblischka, T.H. Johansen, M. Bazilevich, H. Hauglin, H. Bratsberg, B.Ya. Shapiro, Europhys. Lett. **41**, 419 (1998)
3. T.H. Johansen, M. Bazilevich, H. Bratsberg, H. Hauglin, G. Lafyatis, in *High Temperature Superconductors: Synthesis, Processing, and Large-Scale Applications*, ed. by U. Balachandran, P.J. McGinn, J.S. Abell (The Minerals, Metals & Materials Society, New York, 1996), p. 203
4. C.A. Duran, P.L. Gammel, R.E. Miller, D.J. Bishop, Phys. Rev. B **52**, 75 (1995)
5. P. Leiderer, J. Boneberg, P. Brüll, V. Bujok, S. Herminghaus, Phys. Rev. Lett. **71**, 2646 (1993)
6. D. Barness, M. Sinvani, A. Shaulov, T. Tamegai, Y. Yeshurun, Phys. Rev. B **77**, 094514 (2008)
7. T.H. Johansen, M. Baziljevich, D.V. Shantsev, P.E. Goa, Y.M. Galperin, W.N. Kang, H.J. Kim, E.M. Choi, M.S. Kim, S.I. Lee, Europhys. Lett. **59**, 599 (2002)
8. F.L. Barkov, D.V. Shantsev, T.H. Johansen, P.E. Goa, W.N. Kang, H.J. Kim, E.M. Choi, S.I. Lee, Phys. Rev. B **67**, 064513 (2003)
9. M. Marchevsky, L.A. Gurevich, P.H. Kes, J. Aarts, Phys. Rev. Lett. **75**, 2400 (1995)
10. W.W. Mullins, R.F. Sekerka, J. Appl. Phys. **34**, 323 (1963)
11. G.R. Mints, A.L. Rachmanov, Rev. Mod. Phys. **53**, 551 (1981)
12. I. Aranson, A. Gurevich, V. Vinokur, Phys. Rev. Lett. **87**, 067003 (2001)
13. A.L. Rakhmanov, D.V. Shantsev, Y.M. Galperin, T.H. Johansen, Phys. Rev. B **70**, 224502 (2004)
14. I.B. Aranson, B.Ya. Shapiro, V. Vinokur, Phys. Rev. Lett. **76**, 142 (1996)
15. T. Frello, M. Baziljevich, T.H. Johansen, N.H. Andersen, Th. Wolf, M.M.R. Koblischka, Phys. Rev. B **59**, R6639 (1999)
16. M.V. Indebom, H. Kronmüller, P. Kes, A.A. Menovsky, Physica C **209**, 259 (1993)
17. L.M. Fisher, P.E. Goa, M. Baziljevich, T.H. Johansen, A.L. Rakhmanov, V.A. Yampol'skii, Phys. Rev. Lett. **87**, 247005 (2001)
18. A.L. Rakhmanov, L.M. Fisher, A.A. Levchenko, V.A. Yampolskii, M. Baziljevich, T.H. Johansen, JETP Lett. **76**, 291 (2002)
19. P.G. Drazin, W.H. Reid, *Hydrodynamic Stability* (Cambridge University Press, London, 1981)
20. C. Baggio, M. Howard, W. van Saarloos, Phys. Rev. E **70**, 026209 (2004)
21. S. Mohan, Y. Tsuchiya, Y. Nakajima, T. Tamegai, Phys. Rev. B **84**, 180504 (2011)
22. I.S. Aranson, A. Gurevich, M.S. Welling, R.J. Wijngaarden, V.K. Vlasko-Vlasov, V.M. Vinokur, U. Welp, Phys. Rev. Lett. **94**, 037002 (2005)
23. V.V. Bryksin, S.N. Dorogovtsev, Zh. Eksp. Teor. Fiz. **104**, 3735 (1993) [Sov. Phys. JETP **77**, 791 (1993)]
24. L.D. Landau, E.M. Lifshits, *Physical Kinetics* (Pergamon, Oxford, 1991)
25. E.S. Bakhanova, V.M. Genkin, M.A. Kalyagin, S.N. Konkin, S.A. Churin, Zh. Eksp. Teor. Fiz. **100**, 1919 (1991) [Sov. Phys. JETP **73**, 1061 (1991)]
26. D. Chang, B. Rosenstein, C.-L. Wu, Phys. Rev. B **55**, 1162 (1997)
27. D.V. Denisov, A.L. Rakhmanov, D.V. Shantsev, Y.M. Galperin, T.H. Johansen, Phys. Rev. B **73**, 014512 (2006)
28. A.Vl. Gurevich, R.G. Mintz, Rev. Mod. Phys. **59**, 941 (1987)
29. F. Bass, B.Ya. Shapiro, M. Shvartser, Phys. Rev. Lett. **80**, 2441 (1998)
30. F. Bass, B.Ya. Shapiro, I. Shapiro, M. Shvartser, Phys. Rev. B **58**, 2878 (1998)
31. J.S. Langer, Rev. Mod. Phys. **52**, 1 (1980)